Materials Science Forum Vol. 214 (1996) pp. 11-20

Raman Scattering in Materials Science

Z.V. Popovic

Institute of Physics, P.O. Box 57, YU-11001 Belgrade, Yugoslavia

Keywords: Raman Scattering, Phonons, Magnons

ABSTRACT

The use of Raman scattering spectroscopy in the characterization of materials is presented. The representative problems from current literature and our researches are discussed including phase transitions, defects and impurities, magnetic excitations and high-T_c superconductivity.

1. INTRODUCTION

In modern materials science and materials technology the accurately defined structuring of known solids down to microscopically controlled dimensions is now becoming more important than the continual search for new chemical compounds [1]. This trend is most obvious in the domain of semiconductor research and development, but it also applies to other materials, e.g. ceramics and composites, and in a more general sense even to the most recent developments in the field of high-temperature superconductors. The characterization of new structures and materials requires analytical techniques having high sensitivity and accuracy. Raman scattering (RS) spectroscopy is a powerful, non-destructive procedure, sensitive to local environment, ideal for *in situ* probing during growth, and during device fabrication and operation. A variety of fundamental and practical questions have been answered through Raman scattering, like: phases, material quality, collective excitations, defects, carrier characteristics, composition, strains, effects of external perturbations (temperature, pressure, stress, fields) and their gradients [2]. Like X-ray techniques, Raman scattering has become nowadays an indispensable characterization procedure, readily applicable to any bulk material or material system, in numerous disciplines of pure and applied sciences.

2. BASIC OF RAMAN SCATTERING

In principle, all kinds of quasi-particle excitations such as phonons, plasmons, magnons, excitons, polarons and so one can participate in a light scattering process. However, for non-magnetic materials the Raman effect is mostly known as a process involving phonons or electronic excitations. Scattering by phonons occurs in a first or second-order process according to whether one or two phonons interact with the incident photons. The mechanism involves the change of electric polarizability due to atom displacements. In first-order Raman scattering, the incoming photon (frequency ω_L and wavevector k_L) converts into another photon (ω_S,k_S) upon the creation (Stokes process) or the annihilation (Antistokes process) of a phonon according to the well-known energy conservation law:

$$\omega_S = \omega_L \pm \omega_j, \qquad (1)$$

where ω_j is the frequency of the type j-phonon of the crystal; the plus and minus signs correspond to the Antistokes and Stokes processes, respectively.

As a direct consequence of the crystalline periodicity, the momentum conservation law also applies:

$$k_S = k_L \pm q_j, \qquad (2)$$

where q_j is the wavevector of the j-phonon.

The photon wavevector is related to its wavelength through the refractive index n of the medium for the incident or scattered light by

$$k_{L,S} = 2\pi n_{L,S} / \lambda_{L,S} \qquad (3)$$

For a typical backscattering Raman experiment performed in the visible spectral range (500 nm) on absorbing materials ($\alpha > 10^4 cm^{-1}$), the maximum value of $|q_j|$ is well approximated by:

$$|q_j|_{max} = 4\pi n_L / \lambda_L \approx 10^6 cm^{-1} \text{ (using n=4, for GaAs)}$$

Comparing $|q_j|_{max}$ with the range of the phonon wavevectors, i.e. $q < (2\pi/a_o) \approx 10^8 cm^{-1}$ where a_o is the lattice constant, we conclude that only phonons located at, or very near to, the Brillouin zone center can be observed in the first-order Raman scattering.

Experimental RS setup is shown in Fig.1. The light beam provided by a cw laser (typical powers 30-300 mW) is first filtered, then polarized and finally focused onto the sample using cylindrical lens. The scattered light is collected with an objective (aperture better than 1:2) onto the entrance slit of monochromator, which is equipped with holographically ruled gratings with typically 1800 groves/mm. The dispersed light from exit slit of monochromator is usually detected on Peletier-effect-cooled photomultiplier. The final spectra are obtained on computer using photon-counting system integrated in the spectra link (frequency scanning mode). The spectral acquisition time depends on the scattering intensity and may last several hours. In order to reduce the acquisition time and to improve the signal to noise ration the modern Raman scattering systems are equipped with Charge-Coupled-Device (CCD) detectors-devices that consist of two-dimensional diode arrays with micro-electronics processors. More details about these detectors can be found in Ref.[3].

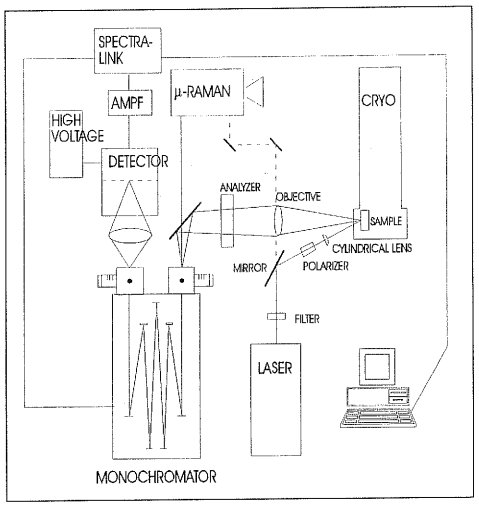

Fig 1. Schematic representation of Raman scattering setup.

3. RAMAN SCATTERING BY PHONONS

As mentioned above, during a light scattering process a quantum of the incident light is annihilated and a quantum of the scattered light is emitted through the creation or annihilation of a crystal excitations. In the case of scattering of light by collective excitations like phonons, the transition electric susceptibility can be expanded in powers of the normal coordinates of the modes. The coefficients of this expansion are the Raman tensors. The differential scattering cross-section by a crystalline excitation with frequency ω is expressed by [4]

$$\frac{\partial^2\sigma}{\partial\Omega\partial\omega} = \frac{\omega_L\omega_S^3}{(4\pi\varepsilon_o)^2c^4}V\left|\mathbf{e}_S\cdot R\cdot\mathbf{e}_L\right|^2\frac{\hbar^2}{2\omega}\left[n(\omega)+1\right]g(\omega) \qquad (4)$$

where V is the scattering volume, $\mathbf{e}_S$ and $\mathbf{e}_L$ are the polarization unit vectors of the scattered and incident light beams respectively, $n(\omega)$ is the Bose-Einstein statistical factor, and $g(\omega)$ a lineshape function (Lorenzian function). Light scattering by a crystalline excitation will be observe only if the quantity

$$\left|\mathbf{e}_S\cdot R\cdot\mathbf{e}_L\right|^2 \neq 0 \qquad (5)$$

where R is the 2nd-rank Raman tensor. Eq.(5) represents selection rules for Raman scattering, which are given in the standard coded form, e.g. x(yz)x; this means that, for incident (scattered) light along the crystal axis x(-x) and polarizations along y(z).

3.1. Raman scattering study of the crystallization and phase transitions

RS is an effective method in investigation of phase transformation in solids, what will be shown in the case of ZrO_2. Zirconium oxide has three well-defined polymorphisms, the monoclinic (space group C_{2h}^5; Z=4), tetragonal (D_{4h}^{15}; Z=2) and cubic (O_h^5;Z=4) structures. The monoclinic phase is stable up to 1100°C and then transforms over a 100°C range to the tetragonal phase. Both of these structures are related to the cubic fluorite structure, which the compound adopts at 2370°C. In monoclinic phase 18 modes are expected to be Raman active. In tetragonal phase 6 modes are Raman active, and in cubic phase only one mode is Raman active. The lattice dynamics of this oxide is given in ref.[6]. In the Raman spectra of polycrystalline ZrO_2 measured with increasing temperatures (Fig.3), the lines show a red shift and an increase in line width as the temperature increases. The spectrum obtained at 1250 K shows a shift of 10 cm^{-1} compared with that obtained at 300 K. At 1430 K, the new structures appear whereas the lines originating from the monoclinic phase become very weak. At 1455 K no striking change appears and 6 Raman lines are to be attributed to the tetragonal phase.

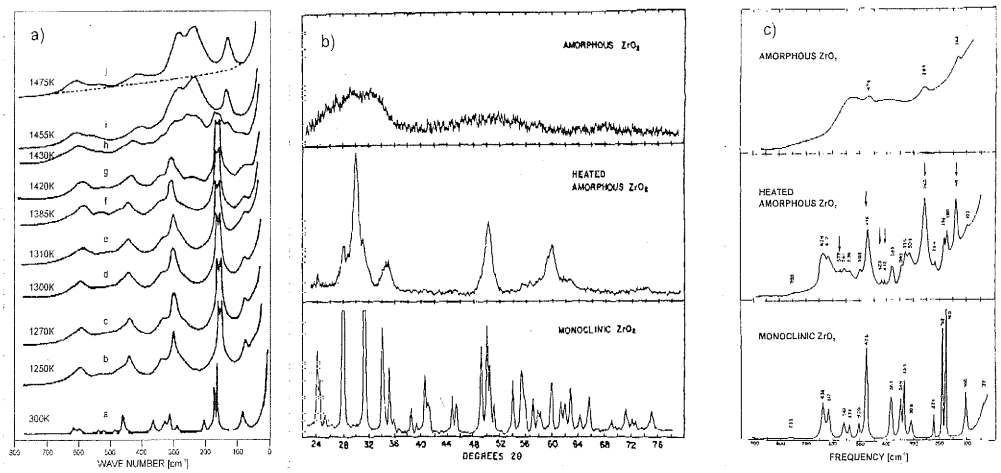

Fig.2. a) Raman spectra of ZrO_2 at different temperatures; b) X-ray diffraction pattern of amorphous, heated amorphous and monoclinic ZrO_2; c) Raman spectra of the same samples as for b).

An illustration of use of Raman spectroscopy in the study of the crystallization of ZrO_2 is given in Fig. 2.a and 2.c. Fig. 2.b shows the X-ray diffraction patterns and Raman spectra of

amorphous, heated amorphous and monoclinic ZrO_2. The x-ray diffraction pattern of amorphous ZrO_2 (Fig.2.b) gives no indication of the presence of crystallinity. Only a very broad peak appears in the vicinity of the strongest peaks of both the tetragonal and monoclinic phases. In comparison, the Raman spectrum exhibits three bands which will be shown to be the strongest peaks of the tetragonal phase. The x-ray diffraction pattern and Raman spectrum of heated amorphous ZrO_2 are also shown in Fig 2.b and 2.c. During heating enough crystallization has occurred for the diffraction pattern to show the 4 major peaks of the tetragonal phase. The broadness of these peaks reflects the fact that crystallization is incomplete. There must also be some monoclinic ZrO_2 in the heated sample, because two strongest peaks of the monoclinic phase are beginning to emerge. Considerably more detailed information can be obtained from Raman spectrum (Fig.2.c), where 20 bands are observed. Comparison with the spectrum of monoclinic ZrO_2 clearly shows that most of these bands result from the presence of monoclinic ZrO_2 in the heated sample. By subtracting those, 3 strong peaks and 3 weak peaks can be attributed to the tetragonal phase.

The main interest of the present study concerns the 3 peaks in the Raman spectrum of amorphous ZrO_2. These frequencies correspond to those of the 3 strongest bands that characterize the tetragonal phase. The observation of distinct vibrations in the Raman spectrum of amorphous ZrO_2 can be interpreted in a way that the atoms are arranged for incipient crystallization and that there must exist interatomic distances similar to those found in tetragonal ZrO_2. When amorphous ZrO_2 is heated, through a diffusionless transformation the interatomic distances change enough for the metastable tetragonal phase to be formed. The tetragonal phase, however, is too unstable to occur as a single phase. Monoclinic ZrO_2, thermodynamically the most stable phase, is invariably formed with the tetragonal form, although in very small amounts.

3.2. Raman scattering by defects and impurities

In Raman spectroscopy, impurities and defects can be observed either via scattering by internal electronic excitations or via scattering by localized vibrational modes. The intensity of the scattered light per unit solid angle $\partial S / \partial \Omega$ can be written as:

$$\partial S/\partial \Omega \approx \sigma \cdot n \cdot V \qquad (6)$$

where σ denotes the scattering cross section per impurity or defect, n is the concentration of scattering centers, and V is the scattering volume. Eq.(6) shows that for a given scattering cross section per impurity or defect and for a given scattering volume, the measured Raman intensity is directly proportional to the impurity or defect concentration. Thus, it is straightforward to calibrate the Raman technique and to make it a versatile tool for quantitative materials characterization.

It is known that, dopant impurities which are significantly lighter than the host lattice atoms give rise to localized vibrational modes (LVM) which are higher in frequency than the intrinsic host lattice phonon modes. The spectroscopy of such vibrational modes is a widely used to analyze residual impurities as well as the incorporation of dopant atoms in semiconductor materials.

The use of Raman spectroscopy for impurity characterization of PbTe (doped with 0,4% In) is given in Fig.3. In PbTe (NaCl type of crystal structure) the first-order Raman modes are not active. At room temperature the modes at 68, 126 and 143 cm^{-1} are clearly observed. These modes are also observed in other telluride compounds and originate from vibrations of TeO_2, a very thin layer regularly created on the surface of the sample. The dominant mode in the spectra of Fig.3 is the mode at 115 cm^{-1}, whose intensity sharply increases as the temperature decreases below 25 K. This temperature is the critical temperature for the appearance of the persistent photoconductivity effect in PbTe(In). As it was discussed in Ref.[8], this mode is In impurity localized vibrational mode which represents a population of metastable In impurity states due to the transfer of electrons from two-electron to one-electron impurity states.

Significant information is contained in the bandshapes of the RS spectra. If for some reasons the lattice does not exhibit translational symmetry, the q=0 selection rule is relaxed and phonons off

the zone center may participate in RS. This is the case in amorphous solids. Thus, Raman spectroscopy becomes a fast and convenient method to determine whether sample under consideration is crystalline or amorphous. In crystalline silicon (c-Si), for example, only the zone center mode at 522 cm^{-1} with a natural linewidth of 3.5 cm^{-1} at room temperature appears. In amorphous silicon (a-Si), the q-selection rule does not apply due to the loss in long range order. All phonons are, therefore, optically allowed and the Raman spectrum resembles the phonon density-of-states with a broad prominent hump at 480 cm^{-1}. Thus the observation of this hump or the sharp line at 522 cm^{-1} differentiates between amorphous and crystalline Si[9].

In some instances spectra intermediate between two extreme cases described above have been reported. They always involve a shift of the 522cm^{-1} line towards lower energy that is accompanied by a broadening. It was further established that the red shift of the 522 cm^{-1} line increases with decreasing crystallite size. In a crystallite assumed to be spherical with a diameter L the phonon is restricted to the volume of the crystallite. In this case, the bandshape of the phonon mode is asymmetrically broadened and can be represented by a Lorentzian convoluted with a Gaussian function of L. With some additional assumptions the scattering intensity takes the form[2]:

$$I(\omega) = \int_0^1 exp(-\frac{q^2 L^2}{4}) \frac{d^3 q}{\left[\omega - \omega(q)\right]^2 + (\Gamma/2)^2} \qquad (7)$$

where q is normalized to $2\pi/a$ and $\omega(q)$ is the appropriate analytical function for the phonon branch in the Brilloiun zone. Eq.(7) is the basis of the spatial correlation model (SCM), which has been successfully applied to a number of physical situations, as will be shown in Fig.4.

Fig.4 (inset) shows an asymmetric spectrum obtained from the micro-crystalline silicon sample (μc-Si). The solid line represents calculated spectra obtained by using the model given by Eq.(7). The best fit parameters are L=40Å, $\Delta\omega$ =1.6cm^{-1} , Γ=5.1 cm^{-1}. Fig.4 shows the relationship between shift and width of the Raman line as well as microcrystallite size in μc-Si sample.

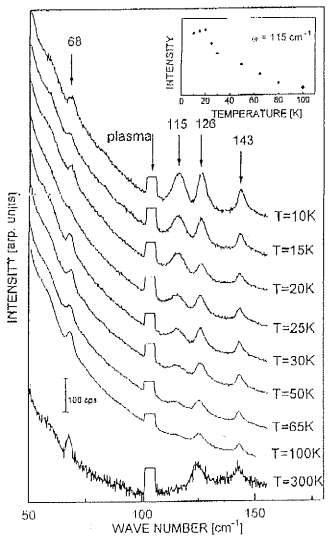

Fig.3. Nonpolarized Raman spectra of PbTe(In) single crystal at different temperatures[8].

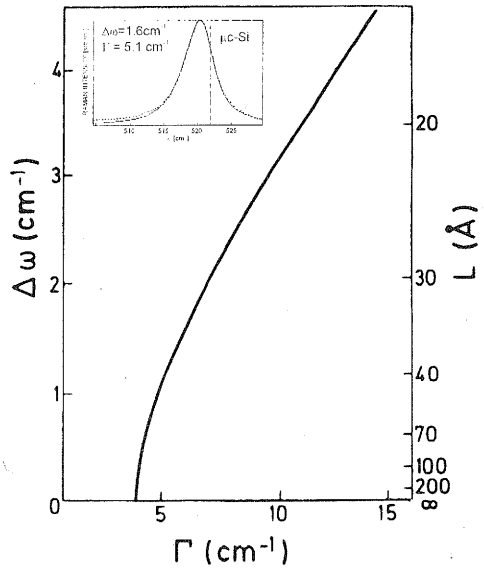

Fig.4. Relationship between shift and width Γ of the Raman line in μc-Si. Inset: Measured (points) and calculated (solid line) Raman line of a μc-Si sample. The dashed vertical line indicates the Raman shift for c-Si[9].

3.3. Raman scattering by phonons in superlattices

Raman-active vibrations in superlattices can be divided into three classifications: confined-optic, folded acoustic and interface modes [10]. Confinement of the optical phonons is a result of the general inability of the two superlattice materials to vibrate in the same optic frequency range, due to different masses of the constituent atoms and/or force constants between them. The vibrations are thus attenuated by the neighboring layers, Fig.5. This leads, in the growth direction, to standing waves with nodes near the material interfaces having wavevectors

$$k_{1,2} = \frac{m\pi}{(n_{1,2}+1)a}, m = \pm 1, \pm 2, \ldots \quad (8)$$

where $d_{1,2}=n_{1,2}a$ is the thickness of the GaAs(1) or AlAs (2) layer. In Eq.(8) the monolayer thickness a has been taken to be the same for both materials. The longitudinal optic (LO) or transverse optic (TO) bands, thus, show Raman scattering from these discrete vibrational states, under the appropriate conditions.

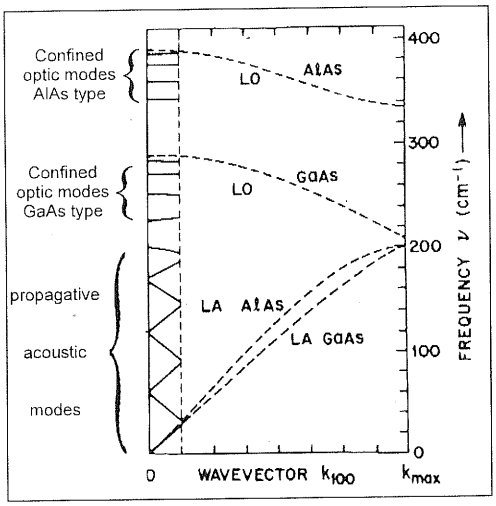

Fig.5. Example of the folding effect in a $(GaAs)_4(AlAs)_4$ SL. Dashed lines stand for the longitudinal dispersion curves in bulk GaAs and AlAs while solid lines represent folded branches according to the new lattice periodicity d along the SL-axis[4].

Because the superlattice imposes a new periodicity with repeat distance $d=d_1+d_2$, the Brillouin zone of the superlattice is folded relative to that of either constituent bulk material. This folding produces phonons with superlattice wavevector $k_{SL}=0$ but with non-zero frequency. These phonons may then participate in normal Raman scattering. The bulk k_B wavevectors which are seen at $k_{SL}=0$ have values

$$k_B = \frac{2m\pi}{(n_1+n_2)a} \pm \frac{4n\pi}{\lambda}, m = 1,2,\ldots \quad (9)$$

the second term representing the backscattering geometry wavevector of the light (n=index of refraction at light wavelength λ). The folded modes are seen in pairs on account of the finite scattering wavevector in Eq.(9) and due to weak repulsion at $k_{SL}=0$, typically separated by $\sim 5cm^{-1}$.

Interface modes in SL appear as a consequence of the discontinuity of dielectric susceptibility at the boundary between two constituent materials.

Many information can be extracted from light scattering experiments performed on superlattices. The study of the folded acoustic modes allows the measurement of the period d through the frequency determination whereas the doublet splittings give more insight into the details of the supercell structure. The quantified optical modes study gives an estimate of the superlattice composition and quality. Furthermore, they are a unique mean of determination of the optical

phonon dispersion curves of crystals like AlAs which are difficult to produce in large volume (necessary for neutron spectroscopy). An illustration of the use of Raman scattering to characterization of superlattice will be given of (311) -oriented GaAs/AlAs superlattice, because for this low-symmetry orientation the folded acoustic phonon modes from all three acoustic branches are Raman active[11] and confined phonon modes show interference and resonance effects [12,13].

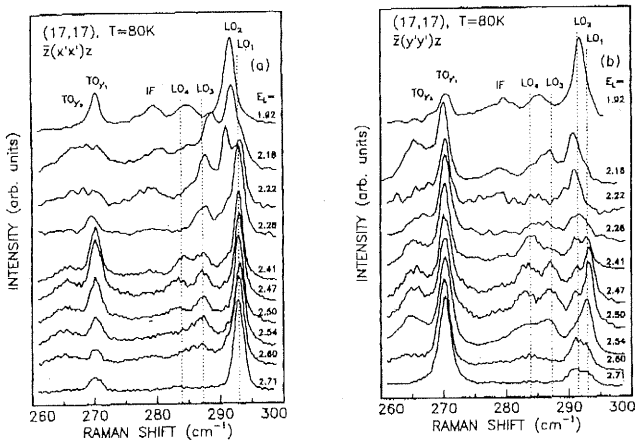

Fig.6. The laser wavelength dependence of the GaAs-like optical phonon Raman spectra of (311)$(GaAs)_{17}(AlAs)_{17}$ SL for (x'x') and (y'y') polarization geometries[12].

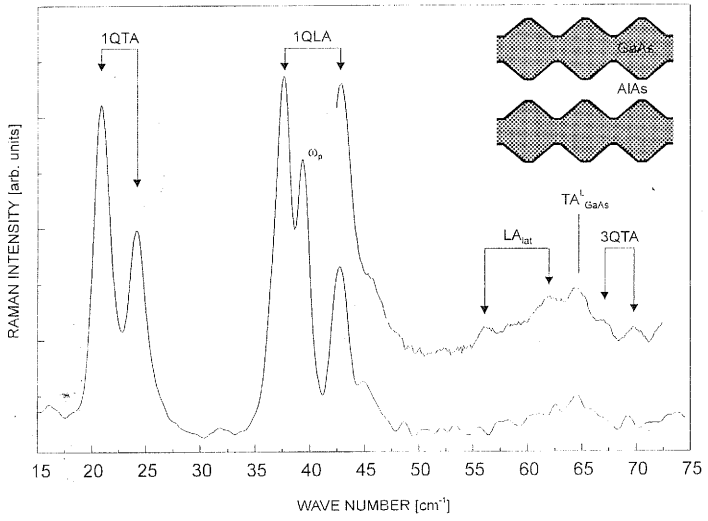

Fig.7.RS spectra of (311) $(GaAs)_{14}(AlAs)_{13}$ SL measured at room temperature with the 488 nm line of an Ar laser [14].

Figure 6 displays the GaAs-like optical modes for the (311) $(GaAs)_{17}(AlAs)_{17}$ SL measured with different lines of argon, krypton-ion, and dye lasers for z'(y'y')z' and z'(x'x')z' polarizations. At the highest laser energy (2.7 eV), the spectra for the two polarizations follow the selection rules; the odd-order TO and LO modes dominate for y'y' and x'x', respectively, with intensities in good agreement with the deformational potential interaction (DPI) Raman tensor for backscattering from the bulk (311) face. At the lowest laser energy in Fig.6 (1.9 eV), the spectra in both polarizations are dominated by the even-order LO modes, indicating the Frohlich interaction (FI) (close with the e1-hh1 band edge transition) to be dominant for these ω_L. For intermediate ω_L's is observed an

intriguing and complex variation of the intensities of the LO and TO confined modes. This behavior is explained as due to interference between the resonant contribution of the hh2-e2 transition of the SL and a background associated with higher energy gaps. The fact that the intensity of the odd order modes resonates demonstrates that the coupling with the hh2-e2 transition is due to DPI in (311) SL's involve intraband phonon scattering in contrast to (100) SL's where only different valence bands can coupled.

Fig.7 shows folded acoustic-phonon Raman scattering spectra of (311) -oriented (311) $(GaAs)_{14}(AlAs)_{13}$ SL. Besides folded phonons from q parallel to the growth direction (1, 3QTA, 1QLA), the folded acoustic-phonon modes from lateral periodicity (LA_{lat}) are observed at frequencies that are in complete agreement with continuum model calculation. It is concluded that the corrugation of (311) surface is present and effective in the sample used.

4. RAMAN SCATTERING BY MAGNONS

Magnetic scattering occurs in paramagnetic materials and in various types of magnetically ordered structure at low temperatures. The magnetic excitations have the form of spin waves or magnons at temperatures lower than the transition temperature of an ordered magnetic material. Magnon frequencies are typically lower than phonon frequencies, and ferromagnets and ferrimagnets always have a very-low-frequency excitation which is best observed by Brillouin scattering techniques. The magnon frequencies in antiferromagnets are usually rather higher and observable by Raman-scattering spectroscopy; most measurements are made on antiferomagnetic crystals.

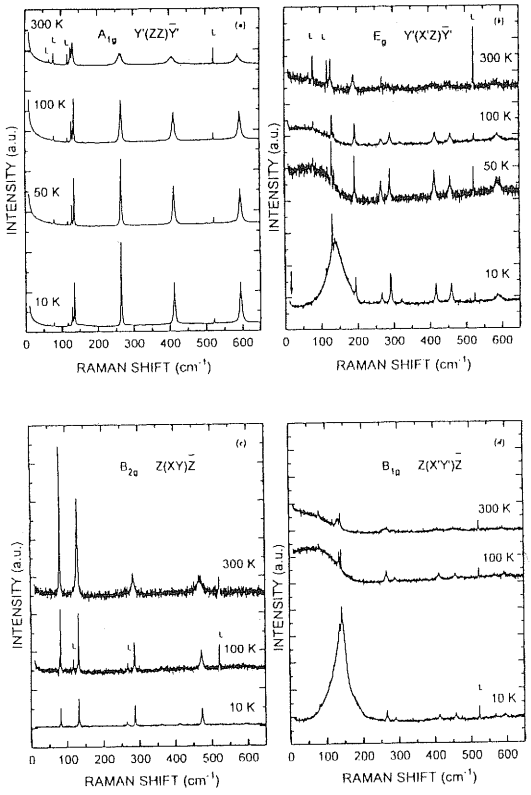

Fig.8. RS spectra at different temperatures for (zz)(A_{1g}), x'z(E_g), (xy)(B_{2g}) and (x'y')(B_{1g}) configuration geometries [17].

The theory of the magnetic-scattering cross section is similar, in principle, to the vibrational case. The main mechanism for the scattering of light by magnons occurs by electric-dipole coupling of radiation to the crystal, and relies on the coupling of spin and orbital motions of the magnetic ions. In order to study the magnetic excitations it is necessary to consider a more general expression of electrical susceptibility that contains spin dependent terms. Detailed analysis can be found in [15]. Further, we give an example of Raman spectroscopy study of magnon excitations in antiferromagnetic Bi_2CuO_4 single crystal. The polarized Raman spectra of the Bi_2CuO_4 single crystal for all principal polarizations at different temperatures are presented in Fig.8. In the magnetic ordered state (bellow 45 K) one wide feature (E_g and B_{1g} symmetry) becomes dominant, which is assigned as two-magnon mode. The small peak denoted by arrow in Fig.8.b comes from one-magnon scattering. The temperature dependencies of these modes are discussed in detail in [16]. It is interesting to note that by using Raman spectroscopy we were able to determine the magnetic moment orientation in this compound. Namely, two directions of the magnetic moments are proposed (along the x and z direction). By analyzing the Raman scattering selection rules from two possible magnetic space groups (orthorhombic and tetragonal) and by comparing the experimental spectra shown in Fig.8, it is concluded that the spin direction is along the z direction[17].

5. HIGH- T_C SUPERCONDUCTORS

Raman spectroscopy is widely used in characterization of high temperature superconducting oxides. The lattice vibrations, phonon mode softening [18], electron-phonon interaction as well as isotopic effect in these oxides are clarified using this technique. For a review see Ref.19.

An illustration of efficiency of Raman scattering in analysis of complex structure of O(4) mode of $YBa_2Cu_3O_{7-x}$ (x=0.6, T_c=35K) is given in Fig.9 [20]. The bandshape appears to vary drastically with laser line frequency ω_L. A consistent three-Lorentzian fit reveals three bands centered at 474, 500 and 488 cm^{-1}. These frequencies do not change with ω_L, but their intensities do, indicating that the three components resonate independently of each other and originate from different crystal phases. The peaks are assigned to the tetragonal (x=1), orthorhombic OI(x=0), and orthorhombic OII phase (x=0.5), all three coexisting within the scattering volume. It is further concluded that, contrary to standard practices, inferring the value of x in such oxygen-deficient crystals from the apparent position of the O(4) Raman mode is not a safe procedure, unless the frequency ω_L is properly taken into consideration.

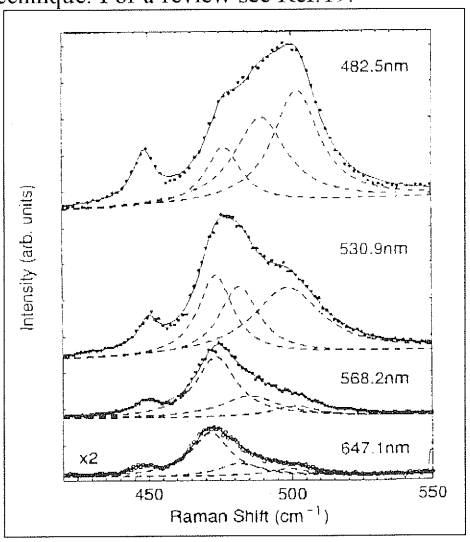

Fig.9. Decomposition of the complex O(4) band of the (zz) spectra at 15K into three Lorentzians and variations of their relative intensity with ω_L.

6. CONCLUSION

Here we pointed out the possibilities of Raman scattering spectroscopy as a powerful characterization technique. The list of possibilities of RS is quite long. Namely, RS is used for investigations of phase transitions, material quality, collective excitations, defects, carrier

characteristics, composition, strains and effects of external perturbations in numerous groups of materials, like semiconductors, ceramics and composites, and high-temperature superconductors.

We thank Dr M.Konstantinovic for critical reading of the text and Mr S.Devic for technical help in manuscript preparation. This work was supported by the Serbian Ministry of Science and Technology under Project No. 0104.

REFERENCES

[1] K.Ploog, Angew.Chem.Int.Ed.Engl.**27**,593(1988).
[2] E.Anastassakis, in *Aplications of Particle and Laser Beams in Materials Technology* (ed. P. Misaelides, Kluwer Academic Publishers, Holland, 1995), p.185
[3] J.C.Tsang, in *Light Scattering of Solids V,* eds. M.Cardona, G.Guntherodt, (Springer Berlin, 1989), p.233.
[4] B.Prevot, J.Wagner, Prog.Crystal Growth and Charact.**22**,245(1991).
[5] E.Anastassakis, B.Papanicolaou and I.M.Asher,J.Phys.Chem.Solids,**36**,667(1975).
[6] M.Ishigame and T.Sakurai,J.Am.Seram.Soc.,**60**,367(1977).
[7] V.G.Karamidas and W.B.White,J.Am.Cer.Soc.,**57**,23(1974).
[8] N.Romcevic, Z.V.Popovic, D.R.Khokhlov,J.Phys.Condens.Mater.**7**,5105(1995)
[9] H.Richter, Z.P.Wang and L.Ley, Solid State Commmun,**39**,625(1981).
[10] B.Jusserand and M.Cardona in *Light Scattering of Solids V,* eds. M.Cardona, G.Guntherodt, (Springer Berlin ,1989), p.49.
[11] Z.V.Popovic, J.Spitzer, T.Ruf, M.Cardona, R.Notzel, and K.Ploog, Phys.Rev.**B48**,1659 (1993).
[12] J.A.Shields, Z.V.Popovic, M.Cardona, J.Spitzer, R.Notzel, and K.Ploog, Phys.Rev.**B49**, 7584 (1994).
[13]Z.V.Popovic, J.Spitzer, M.Cardona, J.A.Shields, R.Notzel, and K.Ploog, Phys.Rev.**B49**, 7577(1994)
[14]Z.V.Popovic, M.Vukmirovic, Y.Raptis, E.Anastassakis, R.Notzel, and K.Ploog, Phys.Rev.**B52**, 5789(1995).
[15]W.Hayes and R.Loudon, *Scattering of Light by Crystals*, (J.Wiley, New York 1978),p.239
[16]M.J.Konstantinovic, Z.V.Popovic S.D.Devic, A. Revcolevschi and G.Dhalenne, J.Phys.: Condens.Matter,**4**,7913(1992).
[17] M.Konstantinovic, Z.V.Popovic, J.Phys.Condens.Mater.**7**,5105(1994)
[18] R.Gajic, S.D.Devic, M.Konstantinovic, Z.V.Popovic, Z.Phys.**B94**,261(1994)
[19] C.Thomsen in *Light Scattering of Solids VI,* eds. M.Cardona, G.Gunterrodt, (Springer-Berlin, 1991), p.285.
[20] M.Iliev, C.Thomsen, V.Hadjiev and M.Cardona,Phys.Rev.**B47**,12341(1993).